Marine and Petroleum Geology 28 (2011) 561–577

Contents lists available at ScienceDirect

Marine and Petroleum Geology

journal homepage: www.elsevier.com/locate/marpetgeo

Downhole well log and core montages from the Mount Elbert Gas Hydrate Stratigraphic Test Well, Alaska North Slope

T.S. Collett [a,*], R.E. Lewis [b], W.J. Winters [c], M.W. Lee [a], K.K. Rose [d], R.M. Boswell [d]

[a] U.S. Geological Survey, Denver Federal Center, MS-939, Box 25046, Denver, CO 80225, USA
[b] Schlumberger, 713 Market Drive, Oklahoma City, OK 73114, USA
[c] U.S. Geological Survey, 384 Woods Hole Road, Woods Hole, MA 02543, USA
[d] U.S. Department of Energy – National Energy Technology Laboratory, Morgantown, WV 26507, USA

ARTICLE INFO

Article history:
Received 9 December 2009
Received in revised form
12 March 2010
Accepted 22 March 2010
Available online 27 March 2010

Keywords:
Gas hydrate
Alaska
Resources
Logs
Core
North Slope
Drilling

ABSTRACT

The BPXA-DOE-USGS Mount Elbert Gas Hydrate Stratigraphic Test Well was an integral part of an ongoing project to determine the future energy resource potential of gas hydrates on the Alaska North Slope. As part of this effort, the Mount Elbert well included an advanced downhole geophysical logging program. Because gas hydrate is unstable at ground surface pressure and temperature conditions, a major emphasis was placed on the downhole-logging program to determine the occurrence of gas hydrates and the in-situ physical properties of the sediments. In support of this effort, well-log and core data montages have been compiled which include downhole log and core-data obtained from the gas-hydrate-bearing sedimentary section in the Mount Elbert well. Also shown are numerous reservoir parameters, including gas-hydrate saturation and sediment porosity log traces calculated from available downhole well log and core data.

Published by Elsevier Ltd.

1. Introduction

Under the Methane Hydrate Research and Development Act of 2000 (renewed in 2005), the U.S. Department of Energy (DOE) has funded laboratory and field research on both Arctic and marine gas hydrates. Among the Arctic studies, BP Exploration (Alaska), Inc. (BPXA) and the DOE have undertaken a project to characterize, quantify, and determine the commercial viability of gas hydrates resources in the Prudhoe Bay, Kuparuk River, and Milne Point field areas on the Alaska North Slope (ANS). In 2005, the analysis of industry acquired 3-D seismic data and existing downhole well log data (enabled by collaborations with the U.S. Geological Survey (USGS) and the Bureau of Land Management (BLM); Lee et al., 2011) identified more than a dozen discrete mapable gas hydrate prospects within the Milne Point area. Because the most favorable of those targets was a previously undrilled, fault-bounded gas hydrate accumulation, BPXA and the DOE decided to drill a vertical stratigraphic test well at that location (named the "Mount Elbert" prospect) to acquire critical reservoir data needed to develop a longer-term production testing program (Hunter et al., 2011). The Alaska, Milne Point area, BPXA-DOE-USGS Mount Elbert Gas Hydrate Stratigraphic Test Well (Mount Elbert Well) was completed in February 2007 and yielded one of the most comprehensive datasets yet compiled on naturally-occurring gas hydrates.

Data collected from the Mount Elbert well, included extensive core-derived sedimentologic (Rose et al., 2011), petrophysical (Winters et al., 2011), and geochemical (Lorenson et al., 2011; Torres et al., 2011) data, downhole open-hole log data (Lee and Collett, 2011), and gas hydrate reservoir engineering data (Anderson et al., 2011). A major component of the Mount Elbert research program was to assess the response of various downhole wireline logging tools to the presence of gas hydrate. Recent advancements in well log evaluation techniques allow for the quantitative assessment of gas hydrate accumulations using conventional downhole well log data (Lee et al., 1996; Collett and Lee, 2005; Kleinberg et al., 2005; Guerin and Goldberg, 2005; Lee and Collett, 2005; Sun and Goldberg, 2005; Lee and Collett, 2011).

The primary goal of this paper is to present a detailed compilation of the downhole well log data from the drilled and cored stratigraphic section in the Mount Elbert well. This paper also contains descriptions and graphical portrayals of numerous well-log-calculated and core-derived reservoir properties. The focus of

* Corresponding author. Tel.: +1 303 236 5731.
E-mail address: tcollett@usgs.gov (T.S. Collett).

0264-8172/$ – see front matter Published by Elsevier Ltd.
doi:10.1016/j.marpetgeo.2010.03.016

this paper is on two large-scale well log montage displays (Figs. 1 and 2) which can be accessed through the online web version of this report at doi:10.1016/j.marpetgeo.2010.03.016. Fig. 1 contains a display of the "general" well-log and core-derived data along with well-log calculated reservoir properties in the Mount Elbert well. Fig. 2 mainly displays "acoustic" well log and core data.

This paper begins with a review of the Mount Elbert operational and well logging program, which is followed by a description of the well log data processing performed before the well log data was used to calculate reservoir properties. The next section of this paper contains a brief description of the well-log inferred gas hydrate occurrences in the Mount Elbert well. The main body of the paper consists of a track-by-track description of the well log data displayed in Figs. 1 and 2. For clarification, the term "track" refers to the data display columns in the enclosed well log montages. The track-by-track descriptions contain discussions pertaining to the source of the portrayed well log and core data, and when applicable, descriptions of the gas hydrate reservoir properties calculated from the available well log measurements. It is important to highlight that all depths noted throughout this paper are measured from the rotary kelly bushing (RKB) on the drilling rig, which was located 55.18 ft (16.8 m) above sea level and 33.78 ft (10.3 m) above the ground surface. In this project all of the downhole log and core data was measured in customary imperial units and for this report have been converted to SI metric units (for all depth measurements it was assumed 1 m = 3.281ft).

2. Well site operations

The Mount Elbert gas hydrate stratigraphic test well was designed as a 22-day program with the planned acquisition of cores, well logs, and downhole reservoir pressure test data. To enable acquisition of high-quality core and downhole log data in a vertical well, the well was spud on February 3, 2007 from a temporary ice pad constructed east of the existing Milne Point Unit E production gravel pad. The surface hole was drilled with water-based mud and with logging-while-drilling (LWD) tools from surface through the permafrost section with a 12 ¼-inch (31.1 cm) bit. On February 8, 9 5/8-inch (24.4 cm) surface casing was set and successfully cemented just below the base of permafrost at a depth of 1952 ft (595 m). The 'main hole' was then drilled using a fit-for-purpose mineral oil-based drilling fluid. Although this choice added both cost and additional operational complexities, the drilling fluid could be kept chilled at or below 0 °C to mitigate the potential for gas hydrate dissociation and hole destabilization and thereby preserve core, log, and reservoir pressure test data quality.

The well was then continuously cored from near the base of the casing to a depth of 2494 ft (760 m) using the Reed Hycalog *Corion* wireline-retrievable coring system. In 23 total deployments, this system successfully recovered 430 ft (131 m) of high-quality 3-inch (7.6 cm) diameter core from 504 ft (154 m) of section (85% recovery efficiency). The coring team processed these cores on site, and collected subsamples for analyses of pore water geochemistry, microbiology, gas chemistry, petrophysical properties, and physical properties. Core samples were also stored in liquid nitrogen or temporarily in pressure vessels for future study of the preserved gas hydrates. Coring operations are discussed in detail in Hunter et al. (2011) and Rose et al. (2011).

After coring, the hole was deepened to 3000 ft (914 m), reamed to a diameter of 8 $^{3}/_{4}$ -inches (22.2 cm), and surveyed with a research-level wireline-logging program including neutron-density sediment porosities, nuclear magnetic resonance, dipole acoustic and electrical resistivity logging, resistivity scanning, borehole electrical imaging, and advanced geochemistry logging (Table 1; Fig. 3). The downhole wireline logging tools as described in Table 1 were provided under a contract with Schlumberger. There were several failed attempts to collect log data with a Sonic Scanner* and Combinable Magnetic Resonance Tool* (CMR); these tool failures were attributed primarily to the effect of the unusually cold borehole conditions. Caliper data indicate that the hole was almost entirely within several centimeters of gauge, and virtually fully in gauge within the gas-hydrate-bearing intervals. This outcome is due largely to the use of oil-based drilling fluid and successful chilling of the drilling fluids with a surface heat exchanger (Hunter et al., 2011).

Following logging, reservoir pressure testing was conducted with the Schlumberger Modular Formation Dynamic Tester* (MDT) at four open-hole stations in two hydrate-bearing sandstone reservoirs (for details on the testing program, see Anderson et al., 2011). Each test consisted of flow and shut-in periods of varying lengths, with one lasting for more than 13 hours. Gas was produced from the gas hydrates in each of the tests.

3. Well log data processing

Schlumberger Well Logging Services was responsible for conducting all of the post-field well log data processing associated with this project, and generated the well log and core data montages as displayed in Figs. 1 and 2.

The quality of the well logs in the gas-hydrate-bearing portion of the Mount Elbert well is excellent. The post-field processing of the log data from the Mount Elbert well consisted of (1) depth adjusting all logs to match gamma ray measurements collected in the logging pass with the Platform Express* (PEX) (Run-2), (2) corrections specific to certain tools for the composition of the drilling mud, (3) processing of the Dipole Shear Sonic Imager* (DSI) and the Combinable Magnetic Resonance Tool* (CMR) logs, (4) special processing of the Rt Scanner* log data, and (5) processing and interpretation of the Oil-Base Microimager* (OBMI) log. Specific tool corrections were performed on the gamma-ray, density, photoelectric, spectral gamma, and neutron porosity data to account for the composition of the drilling fluids. The Dipole Shear Sonic Imager (DSI) post-field processing consisted of interactively extracting compressional- and shear-wave slownesses directly from the field recorded DSI wave-forms. The interactively-picked DSI slowness values were then used to calibrate the full DSI signal array. Well log data quality control consisted of evaluating anomalous and unrealistic values, which resulted in the geologic recognition of several coal zones in the Mount Elbert well.

4. Well log-inferred gas hydrate

Gas hydrates were expected and found in two stratigraphic zones (Figs. 1 and 2), —an upper zone (unit D) containing 44 ft (~13.4 m) of gas-hydrate-bearing reservoir-quality sandstone, and a lower zone (unit C) containing 54 ft (~16.5 m) of gas-hydrate-bearing reservoir. Over 504 ft (154 m) of high quality cores were recovered from the Mount Elbert well between 1990 and 2494 ft (606.5–760.1 m) (Rose et al., 2011). These cores have been the subject of intensive petrophysical examination, the results of which have been used in the well log montages associated with this report to validate and calibrate the acquired downhole log data. The cored and logged gas hydrate occurrences (unit C 2132–2186 ft [649.8–666.3 m] and unit D 2016–2060 ft [614.4–627.9 m]) exhibit deep electrical resistivity measurements ranging from about 50 to 100 ohm-m and compressional-wave acoustic velocities (Vp) ranging from about 3.4 to 4.0 km/s. In addition, the measured shear-wave acoustic velocities (Vs) of the gas-hydrate-bearing

Fig. 1. General well log and core montage for the BPXA-DOE-USGS Mount Elbert Gas Hydrate Stratigraphic Test Well (For interpretation of the references to color in this figure, the reader is referred to the web version of this article.).

horizons in the Mount Elbert well ranged from about 1.1 to 1.8 km/s. Both units displayed gas hydrate saturations that varied with reservoir quality, with typical values between about 50% and 78% of the pore volume. Analysis of core samples indicates that the gas-hydrate-bearing stratigrahic units consist primarily of very fine grained, well sorted, and quartz-rich sandstones (Rose et al., 2011). Core-derived estimates of intrinsic (in the absence of gas hydrate) permeabilities are very high, in the multiple Darcy range (Winters et al., 2011). Porosities are also high, averaging 38% in unit D and reaching 40% within unit C. The NMR log indicates the presence of mobile water, even in the most highly gas-hydrate saturated intervals. In unit D, mobile water may be 8 to 10% of total pore volume. In the case of unit C it appears the mobile water phase may exceed 15% of measured pore volume. The successful depressurization of the reservoir by fluid withdrawal during the MDT program confirms this observation. Analysis of MDT reservoir pressure tests in a variety of advanced reservoir simulators (reviewed by Anderson et al., 2011) has enabled an estimate of 0.12 to 0.17 mD for the in-situ effective permeability of the reservoir in the presence of the gas hydrate phase, which compares favorably to the NMR log derived reservoir permeabilities depicted in Fig. 1.

5. Mount Elbert gas hydrate reservoir properties – general well log and core montage

The well log and core data described in this section are displayed in Fig. 1 (available online at JMPG). The following descriptions are by tracks, labeled T1 through T31 in Fig. 1.

5.1. Track 1

Lithostratigraphy

Two informal stratigraphic units (unit C 2132–2186 ft [649.8–666.3 m] and unit D 2016–2060 ft [614.4–627.9 m]) are interpreted to contain significant amounts of gas hydrate at the site of the Mount Elbert stratigraphic test well (Lee and Collett, 2011; Rose et al., 2011). The cored and logged portion of the Mount Elbert well has been assigned to the Sagavanirktok Formation (Molenaar et al., 1987; Bird, 1998; Rose et al., 2011) and are age-equivalent with the more distal early Eocene marine shales and minor sands of the Mikkelsen Tongue of the Canning Formation further to the east. Using the terminology as proposed by Collett (1993), the Mount Elbert well cored and logged part of units A and E, along with all of units B, C, and D as shown in Fig. 1.

5.2. Track 2

Completion conditions

As shown in Track 2, the Mount Elbert well was first drilled and cased (with a 9 5/8-inch [24.4 cm] diameter casing) to a depth of 1,952 ft (595 m). The 8 3/4-inch (22.2 cm) diameter 'main hole' was cored, reamed, and drilled to a total depth of 914 m (3000 ft). The "main hole" was not cased. Drill pipe conveyed formation pressure testing (MDT test as reviewed by Anderson et al., 2011) were conducted at four depths in the Mount Elbert well as depicted in Track 2: MDT Test C1 – 2161 ft (658.6 m), MDT Test C2 – 2151 ft (655.6 m), MDT Test D1 – 2047 ft (623.9 m), MDT Test D2 – 2025 ft (617.2 m).

5.3. Track 3

Measured depth (1900–3000 ft; 579.1–914.4m)

The subsurface depths used in this display are measured from the rotary kelly bushing (RKB) on the drilling rig, which was located 55.18 ft (16.8 m) above sea level. The original well log data was recorded in feet and later converted to meters as depicted in Track 31 (Fig. 1).

Density standoff (DSOZ) (0–0.5 inches; 0–1.27 cm)

The density standoff is the distance from the density sensor on the Platform Express (PEX) to the borehole wall. Portions of the borehole in which the density sensor did not contact the wall of the borehole are highlighted.

Wireline tension (2000–4000 pound force – lbf)

Wireline tension is the measurement of the downhole tension applied to the logging tool string.

Cable speed (CS) (0–3000 ft/h; 0–914 m/h)

CS in Track 3 is the measured cable speed from the Elemental Capture Spectroscopy Sonde (ECS) tool run (Run-5).

5.4. Track 4

Computed gamma ray (0–150 API)

The computed gamma ray log (CGR) is equal to the total standard gamma ray log count minus the gamma count associated with the occurrence of uranium in the formation. The difference between the spectroscopy gamma ray and computed gamma ray is highlighted (Uranium contribution).

Standard gamma ray (0–150 API)

The standard gamma ray log (SGR) is the total natural gamma ray count measured by the Hostile Natural Gamma Ray Sonde (HNGS) (Run-5).

Borehole drift (0–10 degrees)

The directional drift of the borehole (obtained from the OBMI log, Run-4), both the direction of drift and angle of incline relative to vertical, is shown as a series of 'tadpole' plots. Each tadpole consists of a dot, positioned horizontally to show the angle of incline (0–10°) and the direction of the long tail denotes the borehole drift direction (0–360°). The direction of the short tail denotes the direction of Pad-1 within the hole (0–360°).

Bit size (4–14 inches; 10.2–35.6 cm)

The sub-permafrost gas-hydrate-bearing interval in the Mount Elbert well was drilled and reamed with an 8 3/4 inch (22.2 cm) diameter drill bit.

Caliper (4–14 inches; 10.2–35.6 cm)

The caliper log is a measure of hole diameter as determined from caliper on Platform Express (PEX) (Run-1).

Washout

Portions of the wellbore that are enlarged relative to the size of the drill bit are highlighted as washout zones between the plots of the drill bit size and borehole caliper. As shown, the caliper log measured a near-gauge hole throughout the gas-hydrate-bearing interval.

Mudcake

Portions of the wellbore that are constricted relative to the size of the drill bit are highlighted with increase mudcake between the plots of the drill bit size and the borehole caliper logs.

Rugosity (0–1 events per ft; 0–1 events per 0.30 m)

The rugosity log displays the second derivative of the caliper log with respect to depth from the Platform Express. The units are events per depth.

5.5. Track 5

Array induction resistivity AT10, AT20, AT30, AT60, AT90 (0.2–2000 ohm-m)

The resistivity log traces AT10, AT20, AT30, AT60, and AT90 depict five different measurements of formation electrical resistivities as measured by the Rt Scanner (ZAIT) tool on the Platform Express (Run-1), with AT90 being the deepest reading measurement and AT10 measuring only the shallow formation resistivity. The Rt Scanner (ZAIT) tool has six triaxial arrays, each containing three co-located coils measuring resistivities at various depths into the formation. The high electrical resistivities recorded in the interval from 2016 ft (614.4 m) to 2186 ft (666.3 m) are attributed to the occurrence of in-situ gas hydrate. The apparent overlapping nature of the deep and shallow resistivity logs indicates that the gas-hydrate-bearing formations experienced relatively little drilling disturbance and minimal invasion of mud filtrate.

Apparent formation water resistivity (R_{wa}) (0.2–2000 ohm-m)

The continuous well log plot of pore water resistivity in Track 5 has been derived from the Rt Scanner AT90 deep reading electrical resistivity log. The pore water resistivity log is actually an "apparent" pore water resistivity (R_{wa}) log and it is considered accurate in only water saturated (no hydrocarbons) and clean (shale-free) reservoir-type rocks. Therefore, the apparent pore water resistivities within the log inferred gas-hydrate-bearing units (unit C 2132–2186 ft [649.8–666.3 m] and unit D 2016–2060 ft [614.4–627.9 m]) are not considered accurate where the conditions above are not met. The apparent formation water resistivity (R_{wa}) was calculated with the following equations:

$$R_{wa} = \phi^2 R_t \tag{1}$$

where R_t = deep resistivity; $\phi_{dphi-ecs}$ = density porosity using a ECS-derived matrix density with

$$\phi_{dphi-ecs} = \frac{\rho_{m-ecs} - \rho_b}{\rho_{m-ecs} - \rho_f} \tag{2}$$

where ρ_{m-ecs} = matrix density calculated from geochemical log (see Track 10, Fig. 1), ρ_f = fluid density assumed to be 1.0 g/cm^3 (fresh water), ρ_b = bulk density measured with density log.

Core water resistivity (R_w) (0.2–2000 ohm-m)

Pore water salinities as determined from the analysis of 44 pore water samples collected from the cored interval (1990–2494 ft; 606.5–760.1 m) in the Mount Elbert well (Torres et al., 2011) have been converted to "core measured" water resistivities (shown in Track 5 as individual data points) through the Arps formula (Serra, 1984).

5.6. Track 6

Vertical resistivity (0.2–2000 ohm-m)
Horizontal resistivity (0.2–2000 ohm-m)

The Rt Scanner (ZAIT) triaxial induction tool (Run-1) can be used to calculate vertical and horizontal formation resistivities (R_v and R_h, respectively) as depicted in Track 6. The sections of the borehole in which the Rt Scanner measured vertical resistivities (R_v) are greater than the horizontal resistivities (R_h) have been shaded between the two log curves. For the most part, the measured vertical resistivities (R_v) are greater than the horizontal resistivities (R_h) in the gas-hydrate-bearing sedimentary sections.

5.7. Track 7

Electromagnetic attenuation (0–1000 dB/m)
Electromagnetic propagation time (5–20 ns/m)

The Electromagnetic Propagation Tool* (EPT-G) run with the Platform Express (Run-1) operates at a frequency of 1.1 GHz and measures both the attenuation (EATT) and propagation time (TPL) of an EPT-tool-emitted sinusoidal electromagnetic waves traveling in the formation. In intervals containing gas hydrate, electromagnetic waves propagate like acoustic waves, with faster wave speeds or reduced propagation times (TPL) relative to water-bearing sediments (Sun and Goldberg, 2005). The EATT of a formation, however, is mostly controlled by the porosity or total water content of the formation. Since gas hydrate is mostly composed of water (Collett, 1998), gas hydrate has relatively little affect on the EPT-measured EATT. Thus, the well plot of EATT (brown curve) and TPL (blue) in Track 7 can be used to interpret the presence of gas hydrate. In an EATT-TPL 'cross plot', the log traces are shifted horizontally to overlie one another in water-saturated sand sections. Thus, stratigraphic intervals exhibiting low TPLs and apparent 'crossovers' with the measured EATT (shaded with a stippled green color and labeled "Sand with hydrate") are inferred to contain gas hydrate. The EPT-inferred gas hydrate occurrences compare favorably with those interpreted from other more conventional well log measurements (i.e., electrical resistivity and acoustic transit time) in units C and D. The EATT-TPL 'cross plot' also indicates the presence of gas hydrate in numerous other intervals throughout the borehole. But there is no supporting well log evidence for the occurrence of gas hydrates outside of the resistivity and acoustic transit-time inferred hydrate-bearing sections in units C and D (unit C 2132–2186 ft [649.8–666.3 m] and unit D 2016–2060 ft [614.4–627.9 m]). This apparent discrepancy might be caused by the invasion of oil-based drilling fluids into the formation during drilling which results in a reduced EPT measured propagation time (TPL).

5.8. Track 8

Field neutron porosity (NPHI) (0–80%)

Neutron-derived sediment porosities (thermal neutron porosities assuming sandstone matrix) measured by the Platform Express (PEX) (Run-1) are shown in Track 8 of Fig. 1. This log has been corrected for hole size and standoff only.

Corrected neutron porosity (NPHI-corrected) (0–80%)

Neutron-derived sediment porosities (thermal neutron porosities assuming sandstone matrix) corrected for hole size, standoff, pressure, temperature, mud salinity, and formation salinity are shown in Track 8 of Fig. 1.

Acoustic porosity (SPHI) (0–80%)

Sonic-derived sediment porosities calculated using the Wyllie time-average equation:

$$\phi = \frac{t_{\log} - t_m}{t_f - t_m} \tag{3}$$

where t_{log} = compressional slowness measured with DSI (Run-4); t_m = matrix slowness of 56 μs/ft (sandstone matrix); t_f = fluid slowness of 189 μs/ft (fresh water).

Density porosity (DPHI) (0–80%)

Sediment porosities have been calculated from the bulk density log as measured by the Platform Express (PEX) (Run-1) using the standard density-porosity relation (equation (5)):

$$\phi = \frac{\rho_m - \rho_b}{\rho_m - \rho_w} \quad (4)$$

where ρ_b = bulk density (g/cm^3), ρ_m = matrix density (g/cm^3), ρ_w = water density (g/cm^3).

In equation (4), the density of the formation water (ρ_w) was assumed to be constant and equal to 1.00 g/cm^3 and the matrix (or grain) densities (ρ_m) were calculated from geochemical log (see Track 10, Fig. 1). The density-log-derived porosities in the gas-hydrate-bearing units of the Mount Elbert well, average about 37%.

Total CMR porosity (0–80%)

The Combinable Magnetic Resonance Tool (CMR) deployed (Run-6) in the Mount Elbert well measured the amount of free, not molecularly bound, hydrogen nuclei in the formation—hydrogen in pore water (free and capillary bound), clay-bound water, and hydrocarbons in the pore space. The total CMR porosity log plotted in Track 8 of Fig. 1 includes the contribution from all of the fluid volumes present in the formation. The CMR is insensitive to the hydrogen in the gas hydrate because it is molecularly bound. Total CMR porosities should be similar to both the neutron- and density-log-derived porosities in water-bearing sandstone reservoirs.

Gas hydrate

As discussed in Collett et al. (2005) and shown in the description of Track 14 of Fig. 1, total CMR porosity measurements and density log derived porosities can be used to estimate the concentration of gas hydrate in a rock interval (i.e., from the amount that the density-derived porosity exceeds the CMR porosity). The well log plot 'crossover' of the total CMR and density derived porosities in Track 8 of Fig. 1, highlighted with red hachures, depicts the gas hydrate bulk volume (BV) in the Mount Elbert well as derived from the NMR-density logs.

5.9. Track 9

Formation density (RHOB) (1.5–3.0 g/cm^3)

The bulk formation density measured by the Platform Express (PEX) (Run-1) in the Mount Elbert well is shown in Track 9 of Fig. 1 ('standard' vertical resolution of ~8 inches, 20 cm).

Enhanced resolution formation density (RHOI) (1.5–3.0 g/cm^3)

In addition to the formation density measurement with standard vertical resolution, the Platform Express (PEX) (Run-1) log run in the Mount Elbert well also yielded an "enhanced" resolution formation density log that was recorded with a vertical resolution of about ~2 inches (~5 cm) (Track 9 of Fig. 1).

Density correction (DRHO) (−0.75 to +0.25 g/cm^3)

The compensated litho-density tool, on the Platform Express (PEX) (Run-1) is corrected for adverse borehole and various mud-cake conditions. The calculated density corrections are reported as a log trace and are depicted in Track 9 of Fig. 1.

Photoelectric factor (Pe) – standard resolution (ratio, 0–10)
Photoelectric factor (Pe) – high resolution (ratio, 0–10)

The photoelectric factor log (Pe) in Track 9 of Fig. 1 has been obtained from the compensated litho-density tool on the Platform Express (PEX) (Run-1). In gamma-gamma density logging, gamma rays emitted from a source are scatted by the formation and lose energy until absorbed through the photoelectric effect. The well-log-measured photoelectric effect or factor is a function of the average atomic number of the formation and can yield information about the formation lithology. The two photoelectric factor logs in Track 9 of Fig. 1 have been shown both at 'standard' (~8 inches, ~20 cm) and 'enhanced' (~2 inches, ~5 cm) vertical resolution.

Core bulk density (1.5–3.0 g/cm^3)

Sediment bulk densities determined from nitrogen porosimetry analysis (under in-situ confining pressure conditions) of 20 rock samples collected from the cored interval of the Mount Elbert well (Winters et al., 2011) are shown as discrete values in Track 9 of Fig. 1.

Core gravimetric wet bulk density (MAD) (1.5–3.0 g/cm^3)

Sediment wet bulk densities determined from the analysis of the water content and the mass of the solids in 47 rock samples collected from the cored interval in the Mount Elbert well (Winters et al., 2011) are shown as discrete values in Track 9 of Fig. 1.

5.10. Track 10

Volumetric photoelectric factor (VPE) (0–30 barns/cm^3)

The volumetric photoelectric factor (cross section) of the formation (matrix and fluids), is the product of the photoelectric factor and formation density measured with the litho-density tool on the Platform Express log run (PEX) (Run-1). Note: 1 barn (b) = 10^{-28} m^2.

Apparent volumetric photoelectric factor (VPE-apparent) (0–30 barns/cm^3)

The apparent volumetric photoelectric factor (cross section), depicted in track 10 of Fig. 1, represents a calculated volumetric photoelectric factor of just the matrix. The well log-measured apparent volumetric photoelectric factor provides information about the composition of the formation matrix.

ECS matrix density (ECS-RHOM) (1.5–3.0 g/cm^3)

The ECS-derived matrix density of the formation is calculated using an empirical relationship developed by Herron and Herron (2000) that uses the elemental concentrations from the Elemental Capture Spectroscopy Tool (ECS) (Run-5) as inputs. The following equation was used to produce this log:

$$\rho_{m-ecs} = 2.635 + 0.0439\mathrm{Si} + 0.2277\mathrm{Ca} + 1.992\mathrm{Fe} + 1.144\mathrm{S} \quad (5)$$

The elemental concentrations (Si, Ca, Fe, and S) are in weight fractions.

ELAN matrix density (ELAN-RHOM) (1.5–3.0 g/cm^3)

The ELAN petrophysical software calculates (described in Track 13, Fig. 1) a formation matrix density every 6 in (~15 cm) over the interval evaluated. Each mineral is assigned a matrix density (Table 2), and this value is multiplied by the mineral weight percent to derive the formation matrix density. The calculated matrix density does not include clay-bound water.

Core grain density (CORE-RHOM) (1.5–3.0 g/cm^3)

Core grain densities were determined from grain volume measured by helium injection and dry sample mass of 20 rock samples collected from the cored interval in the mount Elbert well (Winters et al., 2011), are shown as discrete values in Track 10 of Fig. 1.

Core gravimetric grain density (MAD-RHOM) (1.5–3.0 g/cm^3)

Core-derived grain densities determined from helium injection and the dry mass of solids in 47 rock samples collected from the cored interval in the Mount Elbert well (Winters et al., 2011) are shown as discrete values in Track 10 of Fig. 1.

5.11. Track 11

Potassium concentration (0–10 wt %)
Thorium concentration (0–20 ppm)
Uranium concentration (0–10 ppm)

The Hostile Natural Gamma Ray Sonde* (HNGS) deployed in the Mount Elbert well (Runs 5 and 6) uses weighted-least-squares processing algorithms to deconvolve the total gamma spectrum into the three components of naturally occurring gamma-emitting radiation: uranium family, thorium family, and potassium-40. The spectral yield for each element is adjusted to provide a weight percent value. The HNGS also records a standard gamma ray (SGR) and a gamma ray minus the uranium log (CGR) (Track 4; Fig. 1). The spectral yields and computed gamma ray from the HNGS is mainly used to identify mineral types. Note that the concentration of potassium is given in weight-percent, while ppm standards for parts per million.

ECS-derived potassium concentration (0–10 weight percent)

As discussed above, the Hostile Natural Gamma Ray Sonde (HNGS) deployed in the Mount Elbert well (Runs 5 and 6) can be used to calculate the potassium content of sediments. The Elemental Capture Spectroscopy Sonde (ECS) (Run-5) also yields sediment potassium concentrations as shown in Track 11 of Fig. 1. In general, the HNGS- and ECS-derived potassium concentrations compare favorably throughout most of the Mount Elbert well.

5.12. Track 12

SpectroLith weight percents (0 to 100 weight percent)

The Elemental Capture Spectroscopy Sonde (ECS) measures relative elemental yields within the logged formation. SpectroLith (as described by Herron and Herron, 1996) comprises a series of equations that are used to transform the elemental values to mineral and rock weight percents: clay, quartz-feldspar-mica (QFM), carbonate, pyrite, siderite, and coal (Track 12). The chlorite concentration is derived from the ELAN petrophysical model (Track 13) and it is plotted for comparison to XRD core results. These values are plotted in weight percent assuming no porosity. The weight percent iron is plotted from 0 to 25%. The colored red band indicates ±1 standard deviation of the measurement.

XRD core results (0 to 100 weight percent)

The XRD core results (Rose et al., 2011) are plotted as cumulative values to match the SpectroLith log format. These include chlorite, total clay (chlorite + kaolinite + illite + illite/smectite), quartz-feldspar-mica (QFM: quartz + K-spar + plagioclase), carbonate (calcite + dolomite), and pyrite. Carbonate was not detected with XRD so its value overplots the QFM.

5.13. Track 13

Free and capillary bound water (0–100%), carbonate (0–100%), gas hydrate (0–100%), pyrite (0–100%), quartz (0–100%), coal (0–100%), clay-bound water (0–100%), illite–smectite (0–100%), chlorite (0–100%)

To further evaluate the lithology and porosity of the gas-hydrate-bearing sedimentary section in the Mount Elbert well, various well log measurements have been used to construct detailed mineralogic models of the cored and logged sedimentary section at Mount Elbert site. The petrophysical model for the Mount Elbert well was developed with Schlumberger's Elemental Log Analysis* (ELAN) program (Mayer and Sibbit, 1980, Quirein et al., 1986). ELAN is a petrophysical interpretation program designed for depth-by-depth quantitative formation evaluation from wireline logs. ELAN estimates the volumetric fractions of user-defined rock matrix and pore constituents at each depth based on the known log measurement responses to each individual constituent (Table 2). ELAN requires the pre-selection of the volume components present within the formation (i.e., fluids, minerals, and rocks). For each component, the relevant response parameters for each measurement are also required. For example, if it is assumed that quartz is a volume component within the formation and the bulk density tool is used, then the bulk density parameter for this mineral is well known to be 2.65 g/cm^3.

Table 2 lists the well log measurements used to construct the mineralogical models for the sediments at Mount Elbert. When considering the well log data from the Mount Elbert well, the response equations consisted of the expected bulk density, neutron porosity, and iron concentration. The SpectroLith-derived (Track 12) volumes for clay, quartz-feldspar-mica (quartz), carbonate, pyrite and coal were also used as direct inputs to the ELAN model for the Mount Elbert well.

The mineral assemblage that best achieved reasonable results for the log data from the Mount Elbert well, compared to core analyses results discussed in Rose et al. (2011), consisted of carbonate, pyrite, quartz, coal, illite-smectite, and chlorite. The volume of clay-bound water was calculated as product of the volume of clay minerals (illite and chlorite) derived from the ELAN model output, that is each unit volume of illite and chlorite represents the volume of water for a pure clay end point (e.g., 1 volume illite contains 0.125 volume of clay-bound water and 1 volume of chlorite contains 0.10 volume of clay-bound water).

The gas hydrate content in Track 13 (Fig. 1) was solved outside of the ELAN-Plus model by direct calculation from the NMR-density porosity technique (Fig. 1, Track 14). The NMR-density-porosity-derived gas hydrate saturations were converted to weight fraction (*WHYD*) by the following equation:

$$WHYD = \frac{\left(\phi_{dphi-ecs} - \phi_{TCMR}\right)}{\rho_b}\rho_{hydrate} \quad (6)$$

where $\rho_{hydrate}$ = gas hydrate grain density (0.91 g/cm^3); ρ_b = bulk density from log (g/cm^3); $\phi_{dphi-ecs}$ = density porosity calculated using ECS-derived matrix density (%); ϕ_{TMR} = total CMR porosity (%).

Note that in ELAN, the input values for weight percent of each component range from 0 or 1, with 1 equal to unity or 100%. The input log data for the volume of quartz, carbonate, pyrite, clay, and coal (along with and their respective weight percents) were calculated from the Elemental Capture Spectroscopy Sonde* (ECS) using the SpectroLith* methodology (Herron and Herron, 1996). These values are shown in Track 12 (Fig. 1). The SpectroLith weigh percent values (0 or 1) are used to constrain the calculated mineral or rock volumes into the appropriate predicted rock or fluid bin. For example, clay weight percent is assigned to both chlorite and illite but not to any of the other volumes.

5.14. Track 14

Gas hydrate saturation (CMR-DEN) (0–100%)

As discussed in the description of Track 8 (Fig. 1) and reviewed in Lee and Collett (2011), total CMR-porosity measurements and density-log-derived porosities can be used to estimate the concentration of gas hydrate in a rock interval. The well log plot crossover of the total CMR and density-derived porosities in Track 8 of Fig. 1, highlighted with red hachures, depicts the gas hydrate bulk volume (BV), which has been plotted in Track 14 (Fig. 1) as a CMR-density porosity-derived gas hydrate saturation log (i.e., the percent of pore-space occupied by gas hydrate).

Gas hydrate saturation (compressional-wave) (0–100%)
Gas hydrate saturation (Shear-wave) (0–100%)

As described by Lee and Collett (2011), compressional- and shear-wave slowness data from the Dipole Shear Sonic Imager (DSI) (Run-4) can be used to calculate gas hydrate concentrations, included in Track 14 (Fig. 1).

Gas hydrate saturation (Resistivity) (0–100%)

As described by Lee and Collett (2011), electrical-resistivity well-log data measured by the Platform Express (PEX) (Run-1) can also be used to calculate gas hydrate concentrations, included in Track 14 (Fig. 1).

Gas hydrate saturation (ELAN) (0–100%)

As described in the discussion of Track 13 (Fig. 1), ELAN-Plus (Elemental Log Analysis) petrophysical modeling was also used to estimate gas hydrate saturations in the Mount Elbert well. This estimate is derived by the CMR-density hydrate saturation method, but in this calculation it is allowed to vary in response to other log measurements in the ELAN model.

Core-derived gas hydrate saturation (Core S_h linear) (linear Cl^- relationship) (0–100%)
Core-derived gas hydrate saturation (Core S_h diffusion) (diffusion Cl^- relationship) (0–100%)

Pore-water freshening in recovered conventional cores (i.e., not pressure cores) have been used to estimate gas hydrate saturations in numerous marine and permafrost-associated gas hydrate studies (Tréhu et al., 2004; Tomaru et al., 2005). Torres et al. (2011) have also used core-derived pore-water chlorinity freshening trends to estimate gas hydrate saturations in the cored section of the Mount Elbert well. Depicted in Track 14 (Fig. 1) as discrete data points are two sets of 63 chlorinity (Cl^-) derived gas hydrate saturation estimates, with one set assuming a linear background relationship and the second assuming a water chemistry profile that has been modified by permafrost formation as described by Torres et al. (2011). Gas hydrate saturations estimated from the core-derived chlorinity trends agree with most of the downhole log-derived estimates when the gas hydrate occupies more than 20% of the pore space; however, the correlation in the stratigraphic section just below the unit C and D well-log-inferred gas hydrate occurrences is less robust. Reasons for this discrepancy are still unclear, but may reflect problems associated with the accurate selection of baseline reservoir conditions or pore-fluid chemistries in a complex sedimentary section.

5.15. Track 15

Gas hydrate saturation (EPT) (0–100%)

Electromagnetic propagation well log (Run-1, EPT-G) data was used to measure in-situ dielectric properties of natural gas hydrate in the Mount Elbert well (Fig. 1, Track 7). Sun et al. (2011) were able to calculate gas hydrate saturations from the derived dielectric constants and density logs. The gas hydrate saturation log derived from the NMR-density porosity method (Track 14, Fig. 1) has also been included in Track 15 (Fig. 1) for comparison purposes. The electromagnetic log yields similar gas hydrate saturations to the NMR-density log-derived values within the portions of units C and D sands that were inferred to contain gas hydrate from other well log measurements (i.e., electrical resistivity and acoustic transit time). The electromagnetic-log-derived gas hydrate saturations, however, remain highly variable and often high throughout most of the logged section depicted in Track 15 of Fig. 1 (EPT-derived gas hydrate saturation log is truncated below a depth of 2220 ft [677 m]). The reason for the apparent discrepancy between the electromagnetic-log-derived gas hydrate saturations and all of the other downhole-log-derived gas hydrate saturations as depicted in Tracks 14 and 15 of Fig. 1 is not known. As discussed in Track 7, however, this apparent discrepancy might be caused by the invasion of oil-based drilling fluids into the formation during drilling which results in a reduced EPT measured propagation time TPL. It is reasonable to assume that the highly variable electromagnetic-log-derived gas hydrate saturations, outside of the well documented unit C and D gas hydrate occurrences, are likely erroneous.

Gas hydrate saturation (CMR-DEN) (0–100%)

The CMR-density-derived gas hydrate saturation log plot from Track 14 (Fig. 1) has been included in Track 15 (Fig. 1) for comparison purposes.

5.16. Track 16

Formation temperature (25 to 75 °F, −4 to 24 °C)

Plotted in Track 16 of Fig. 1 is a borehole equilibrated formation temperature profile, as measured in the Milne Point Unit D-2 well (http://esp.cr.usgs.gov/data/bht/alaska/), which is located ~2 miles (~3.2 km) north of the Mount Elbert well.

Hydrostatic pressure (0–2000 psi, 0–13,790 kPa)

Limited pore pressure data from onshore wells on the Alaska North Slope suggest near hydrostatic pore pressure conditions immediately below the base of permafrost (Collett, 1993). Therefore, an assumed hydrostatic pore pressure gradient of 0.433 psi/ft (9.795 kPa/m) is plotted in Track 16 of Fig. 1.

Gas hydrate stability zone

Also shown in Track 16 of Fig. 1 is the depth limit (2853 ft; 869.6 m) of the gas hydrate stability zone.

5.17. Track 17

Total gas (0–5000 Units)
Methane (0–250,000 ppm)

Track 17 of Fig. 1 contains a 'total gas' log and the gas chromatographic log of methane from the mud log report for the Mount Elbert well (Hunter et al., 2011). The total gas log is plotted in mud logging 'Units', while the gas chromatographic data is reported in parts per million (ppm). The mud gas log of both total gas and methane appear to be shifted downward from the resistivity and acoustic log inferred gas hydrate occurrences in units C and D. The reason for this apparent depth shift is unknown; however, it cannot be easily attributed to a drilling fluid return lag-time calculation error because the magnitude of the shift is too great.

5.18. Track 18

Total CMR porosity (0–60%)
CMR porosity >3 ms (0–60%)
CMR free fluid (0–60%)

As discussed above in the description of Track 14 (Fig. 1), the NMR-recorded transverse-magnetization-relaxation time (T_2) of a formation depends on the relaxation characteristics of the hydrogen-bearing substances in the rock formation. For example, T_2 for hydrogen nuclei in solids is very short, whereas T_2 for hydrogen nuclei in fluids can vary from tens to hundreds of milliseconds, depending on fluid viscosities and interactions with nearby surfaces. In standard NMR borehole logging, the T_2 relaxation signal is divided into a series of time windows, with each

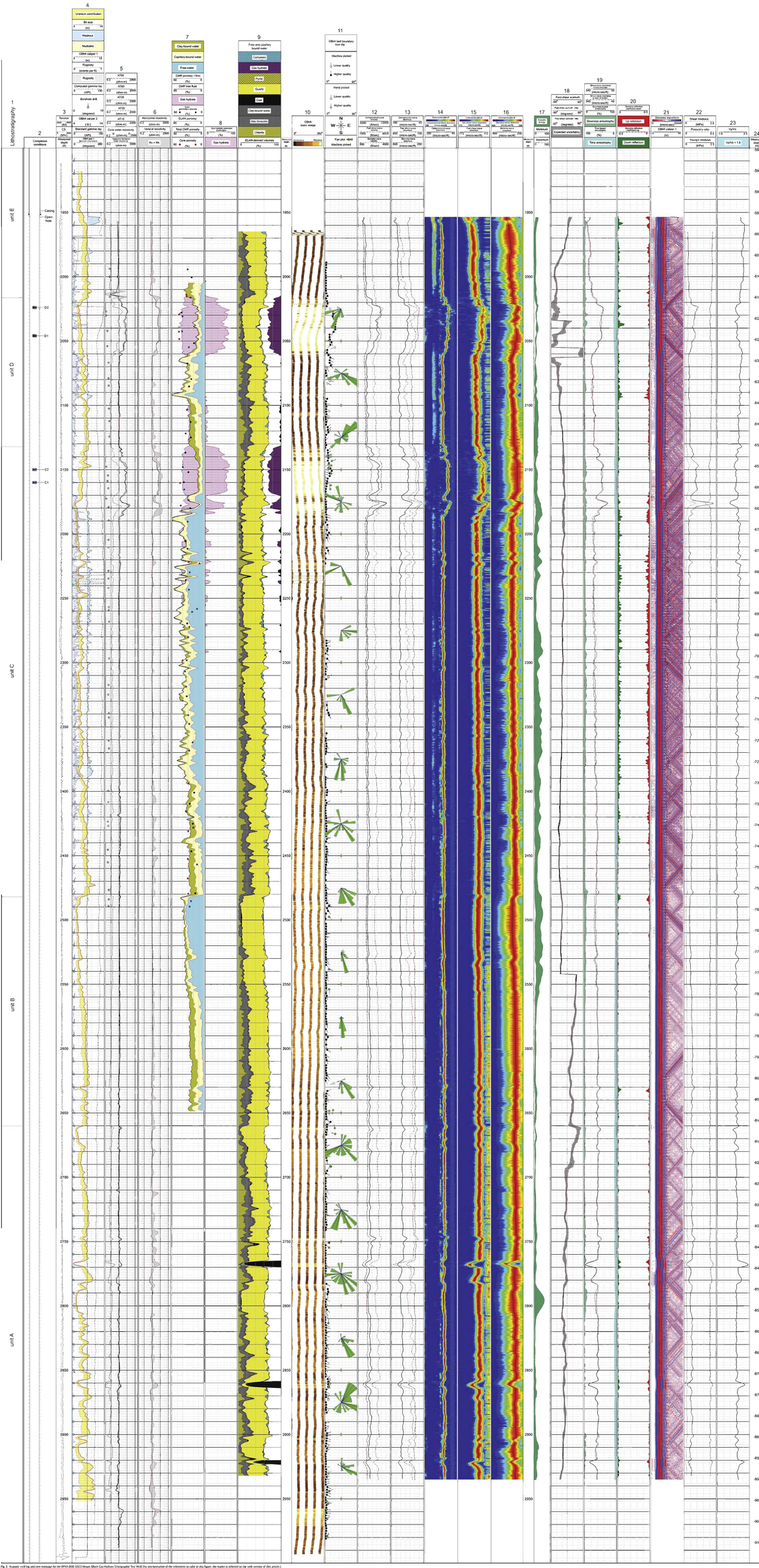

Fig. 7. Acoustic well log and core montage for the BPXA-DOE-USGS Mount Elbert Gas Hydrate Stratigraphic Test Well (the interpretation of the reflectors in color in this figure, the reader is referred to the web version of this article).

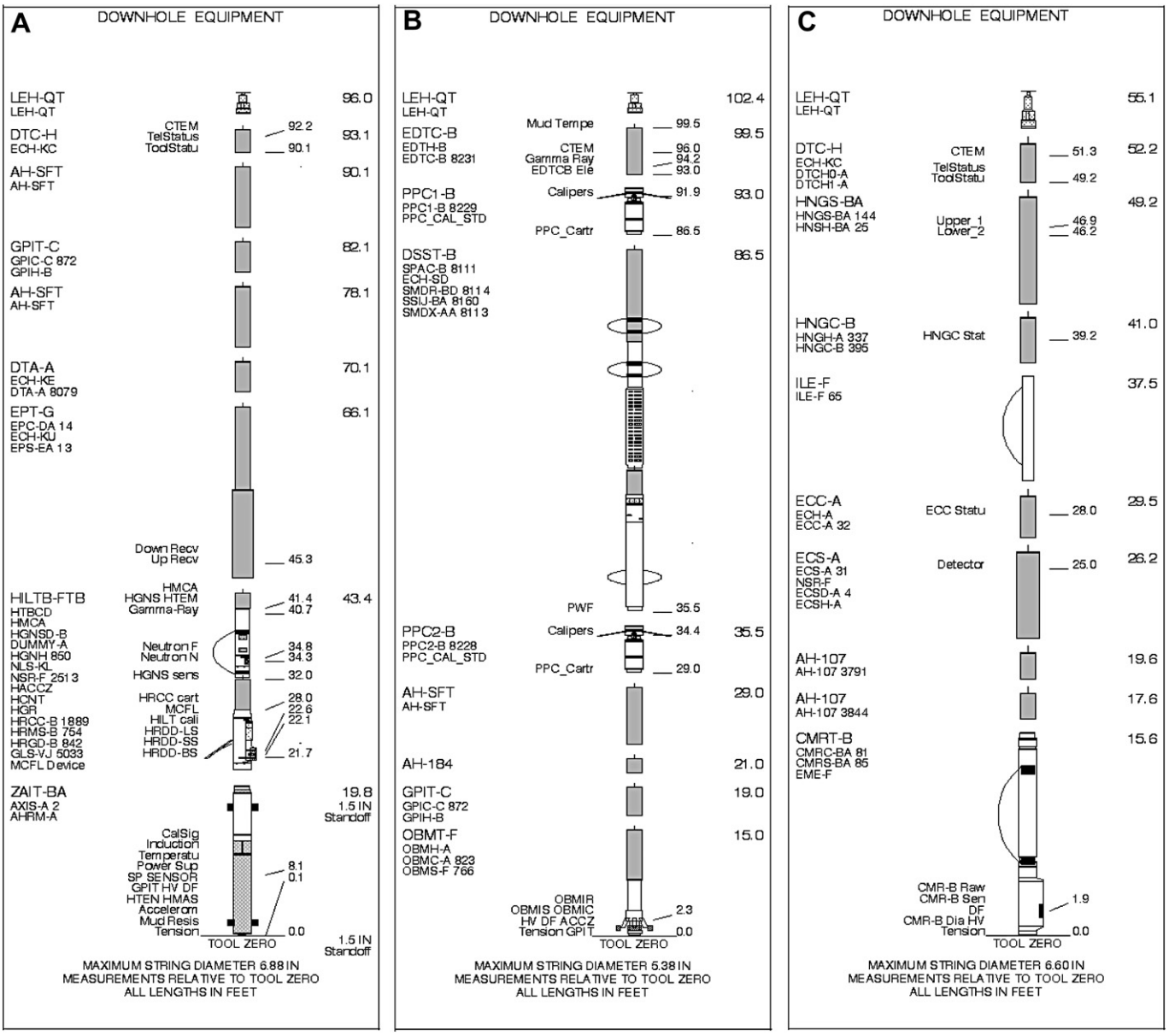

Fig. 3. Schematic diagram of Schlumberger logging tool strings used in the sub-permafrost section of the BPXA-DOE-USGS Mount Elbert Gas Hydrate Stratigraphic Test Well: (a) Run-1: Platform Express (PEX/HILTB), RT-Scanner (ZAIT), Electromagnetic Propagation Tool (EPT-G), Gamma Ray Log (GR), Litho Density, Compensated Neutron Porosity (CNT), General Inclinometry Tool (GPIT), High-Resolution Mechanical Sonde (HRMS); (b) Run-4: Dipole Shear Sonic Imager (DSI/DSST-P), Oil-Base Microimager Tool (OBMI), General Inclinometry Tool (GPIT), Gamma Ray Log (GR); (c) Runs-5 and -6: Combinable Magnetic Resonance Tool (CMR), Hostile Natural Gamma Ray Sonde (HNGS), Elemental Capture Spectroscopy Sonde (ECS). Most of the acronyms used on the tool schematics have been further defined in Table 1, additional information about each tool can be found on the following web site http://www.slb.com/modules/mnemonics/index.aspx.

representing a portion of the T_2 signal that can be attributed to the various 'types' of water within a porous rock unit (i.e., clay-bound water, capillary-bound water, and free water). Generally, clay-bound water is believed to be characterized by T_2 relaxation times ranging from 0.3 to 3 msec (shown as the water volume between the plot of total CMR porosity and CMR porosity >3 ms, shaded in olive-green in Track 18 of Fig. 1). The T_2 relaxation time for capillary-bound water in Track 18 (Fig. 1) falls between the plot of the CMR porosity >3 ms and the CMR free fluid porosity, which is shaded yellow. The volume of mobile free-water in the formation is depicted by the plot of the CMR free fluid porosity log and has blue shading. The T_2 cutoff between free water and capillary-bound water was estimated to be 33 ms, a typical value for a sandstone reservoir.

5.19. Track 19

T_2 amplitude distribution (relative scale, 0–29)
T_2 cutoff (0.3–3000 ms)
T_2 logarithmic mean (0.3–3000 ms)

As discussed in the descriptions of Tracks 14 and 18 (Fig. 1), one of the primary functions of NMR downhole logging tools are to measure the signal associated with the transverse relaxation time, T_2. The plot of the T_2 amplitude distribution in Track 15, highlighted in green, depicts the CMR-recorded (Run-6) T_2 signal amplitudes as a function of relaxation time. It is calculated every 6-in in the log processing but displayed every 3-ft in this track. The plot of the T_2 logarithmic means in Track 15 (orange curve) represent the logarithmic mean value of the recorded T_2 relaxation time for each

Table 1
Logging while drilling (LWD) and open hole well logging program in the BPXA-DOE-USGS Mount Elbert Gas Hydrate Stratigraphic Test Well.

BPXA-DOE-USGS Mount Elbert Gas Hydrate Stratigraphic Test Well Logging Program			
Run Number	Date	Logged interval (ft)	Logging tool
LWD	February 4–15, 2007	275-3000	Drilling performance, Gamma Ray Log (GR), EWR-Resistivity, Neutron Porosity, Density (only GR below 1960 ft)
1	February 14, 2007	1952–2994	Platform Express (PEX/HILTB), Rt-Scanner (ZAIT), Electromagnetic Propagation Tool (EPT-G), Gamma Ray Log (GR), Litho Density, Compensated Neutron Porosity (CNT), General Inclinometry Tool (GPIT), High-Resolution Mechanical Sonde (HRMS)
2	February 14, 2007	No data recorded	Sonic Scanner (MSIP), Oil-Base Microimager Tool (OBMI), General Inclinometry Tool (GPIT), Gamma Ray Log (GR) - MSIP failed no log data collected
3	February 14, 2007	No data recorded	Dipole Shear Sonic Imager (DSI/DSST-P), Oil-Base Microimager Tool (OBMI), General Inclinometry Tool (GPIT), Gamma Ray Log (GR) - DSST-P failed no log data collected
4	February 14, 2007	1952–2944	Dipole Shear Sonic Imager (DSI/DSST-P), Oil-Base Microimager Tool (OBMI), General Inclinometry Tool (GPIT), Gamma Ray Log (GR)
5	February 14, 2007	1952–2974	Combinable Magnetic Resonance Tool (CMR), Hostile Natural Gamma Ray Sonde (HNGS), Elemental Capture Spectroscopy Sonde (ECS) - CMR failed, logged up with only the ECS/NGT
6	February 14, 2007	2000–2648	Combinable Magnetic Resonance Tool (CMR), Hostile Natural Gamma Ray Sonde (HNGS)

discrete measurement. This values is used as an input into the estimation of the SDR permeability in Track 21. The T_2 cutoff shows the boundary between free water (right of cutoff) and capillary-bound water (left of cutoff). This value was estimated to be 33 ms, a typical value for a sandstone reservoir.

Core-derived T_2 logarithmic mean (0.3–3000 ms)
Core-derived T_2 cutoff (0.3–3000 ms)

Winters et al. (2011) measured the T_2 cutoff values in four core samples using a laboratory NMR system (red dots). The logarithmic mean for these samples is 36.7 ms. Winters et al. (2011) also measured the T_2 mean in the laboratory, and water-saturated values were measured with an echo spacing of 0.6 ms (plotted as gold dots).

5.20. Track 20

Combinable magnetic resonance (CMR) bin porosities 1–8 (0–60%)

As discussed in the description of Tracks 14, 18, and 19 (Fig. 1), NMR downhole log data can be used to measure the NMR relaxation characteristics of hydrogen-bearing fluids in a rock section, which can in turn be used to further analyze the nature and size of pores in the NMR logged section. A series of CMR derived 'bin' porosities (from 1 through 8) are plotted in Track 20, each of which represent a portion of the T_2 relation signal shown in Track 19. Each of the bins represents a different time range within the entire recorded spectrum: Bin-1 (0.3–1.0 ms), Bin-2 (1.0–3.0 ms), Bin-3 (3.0–10.0 ms), Bin-4 (10.0–30.0 ms), Bin-5 (30.0–100.0 ms), Bin-6 (100.0–300.0 ms), Bin-7 (300.0–1000.0 ms), and Bin-8 (1000.0–3000.0 ms). Bin 1 (shaded in magenta) represents the shortest relaxation time; Bin 8 (shaded in orange) represents the longest relaxation time.

5.21. Track 21

Density porosity (DPHI) (0–60%)
Total CMR porosity (0–60%)

The density-log-derived and total CMR sediment porosities described in Track 8 (Fig. 1) have been included in Track 21 (Fig. 1) for comparison purposes with other log- and core-derived sediment porosities.

ECS density porosity (0–60%)

The Elemental Capture Spectroscopy Sonde (ECS) density-derived porosity was calculated using the ECS-estimated matrix density displayed in Track 10 (Fig. 1).

ELAN porosity (0–60%)

The ELAN porosity is the effective porosity calculated using the parameters presented in Table 2 and described in Track 13 (Fig. 1). This volume represents the total porosity less the clay-bound water. In non-hydrate bearing zones it will be slightly lower value than the density log porosities because the density log is not able to differentiate between total and effective porosity.

Core porosity (0–60%)

Sediment porosities, as determined from nitrogen porosimetry analysis (under in-situ confining pressure conditions) of 20 rock samples collected from the cored interval of the Mount Elbert well (Winters et al., 2011), are shown as discrete values in Track 21 of Fig. 1.

Core gravimetric porosity (MAD) (0–60%)

Sediment porosities, as determined from the analysis of the water content and the mass of the solids in 47 rock samples collected from the cored interval in the Mount Elbert well (Winters et al., 2011), are shown as discrete values in Track 21 of Fig. 1.

5.22. Track 22

Combinable magnetic resonance (CMR) SDR permeability (0.01–10,000 mD)
Combinable magnetic resonance (CMR) timur/coates permeability (0.01–10,000 mD)

Another primary goal of NMR downhole logging is to measure the permeability of rocks to the flow of various formation fluids. Two empirical relations have been developed to use CMR-derived NMR log data to predict in situ fluid permeabilities: the SDR and Timur/Coates methods (Horkowitz et al., 2002) as shown in Track 22 (Fig. 1). Note that 1 mD $\approx 10^{-15}$ m^2.

ELAN permeability (0.01–10,000 mD)

Within the ELAN model, described in Track 13 (Fig. 1), the intrinsic permeability shown in Track 22 was calculated following a mineral-to-permeability relationship proposed by Herron (1987) in which model-derived mineral assemblages are used to calculate permeabilities.

Core permeability – minipermeameter (0.01–10,000 mD)

A laboratory minipermeameter, developed by the University of Alaska at Fairbanks, was used to measure sediment permeabilities

on 658 frozen core samples from the Mount Elbert well (no gas hydrate was preserved in the cores); these data are shown as discrete values in Track 22 of Fig. 1. This contact measurement tool uses air to measure the permeability of the sample without any confining pressure.

Core nitrogen permeability at confining pressure (0.01–10,000 mD)

Laboratory measured sediment permeabilities to nitrogen gas under confining pressure conditions were determined for 20 core samples that did not contain gas hydrate when analyzed in the laboratory (Winters et al., 2011); these data are shown as discrete values in Track 22 of Fig. 1.

Core Klinkenberg permeability at confining pressure (0.01–10,000 mD)

Klinkenberg permeabilities are calculated from laboratory permeability tests under confining pressure conditions using nitrogen. A total of 20 Klinkenberg permeabilities were calculated (Winters et al., 2011); these data are shown as discrete values in Track 22 of Fig. 1.

5.23. Track 23

Core sediment log

Track 23 contains a graphical depiction of the major core-derived sediment types as described in Rose et al. (2011). For the complete lithostratigraphic montage and more information on the color coding and symbols used in the core sediment log see the 'explanation' associated with the sediment log in Rose et al. (2011).

5.24. Track 24

Core samples: clay size (0–100%), silt size (0–100%), and sand size (0–100%)

Sediment grain size (i.e., clay, silt, and sand size), as determined by laser light diffraction analysis of 134 sediment samples collected from the cored interval in the Mount Elbert well (Winters et al., 2011), is shown both as discrete values (i.e., core points) and as log traces in Track 24 of Fig. 1. An additional 273 sediment grain size measurements, also using laser light diffraction analysis, were conducted as part of the detailed lithostratigraphic description of the core by Rose et al. (2011); these analysis are shown as only discrete values (i.e., core points).

5.25. Track 25

Oil-base microimager tool (OBMI) dynamic image

The Oil-Base Microimager Tool (OBMI) (Run-4) produces oriented electrical images of the borehole wall in nonconductive (oil-base) mud. This can be used for detailed sedimentological and structural interpretations (Amer and Alexander, 2005). It is also possible to use the OBMI to obtain high-resolution electrical images of gas hydrates in the wellbore, thus yielding information about the nature and texture of gas hydrate occurrence in a rock interval. The OBMI tool has four pads that contain five pairs of electrodes on each pad face, with a vertical image resolution of 0.5 inch (~1.3 cm) and image coverage of ~32% in a 8.0 inch (~20.3 cm) borehole. The OBMI has a shallow depth of investigation of ~4.0 inches (~10.2 cm), which may theoretically allow the OBMI to directly measure in-situ gas hydrates. AC current is focused into the formation from each pair of electrodes. The voltage drop across the pair is used to quantify formation microresistivity. The computed values for each electrode pair, which reflect microresistivity variations of the formation, are converted into high resolution brown-scale (or color) images of variable intensity. Black and yellow (or darkest and lightest color) indicate the low and high microresistivity respectively. The OBMI tool string contains a General Purpose Inclinometry Tool* (GPIT) that orients the resistivity measurements through the use of an accelerometer and magnetometer responding to the declination and inclination of the Earth's magnetic field. The raw data are processed in real-time during logging to transform individual microresistivity traces into oriented images. Detailed processing and interpretation of the OBMI resistivity images in combination with other log and core data was carried out in post-field studies by Schlumberger Well Logging Services.

To further assess the nature of in-situ gas hydrate occurrences, the OBMI images from the interval of well log-inferred gas hydrates in the Mount Elbert well were reprocessed and examined. The OBMI image in Track 25 (Fig. 1) was generated with GeoFrame* software, a Schlumberger well log data processing package. OBMI log processing followed standard procedures that included, among other, a series of logging tool speed corrections. The OBMI image in Track 25 (Fig. 1) was generated in 'dynamic' mode, where the image is normalized such that all 42 shades of yellow to black are depicted within an approximately 2 ft (~0.6 m) sliding depth window. Dynamic normalization permits the depiction of fine sedimentary structures within zones that have limited differences in electrical conductivity. The OBMI image is characterized by light colored (high resistivity) to dark colored (low resistivity) bands, which in many cases can be traced across the entire display. These continuous bands likely represent distinct stratigraphic units with thicknesses ranging between 4–20 inches (~10.2–50.8 cm). The OBMI imaged light colored stratigraphic beds within the hydrate-bearing portions of units C (2132–2186 ft; 649.8–666.3 m) and D (2016–2060 ft; 614.4–627.9 m;) are likely intervals of relatively high gas hydrate saturations.

5.26. Track 26

Oil-base microimager tool (OBMI) bed boundary true dip

The Oil-Base Microimager Tool (OBMI) (Run-4) data were evaluated to identify and characterize sedimentary bed boundaries. Bed orientation was computed over the entire logged interval through an automated process that correlates features in microresistivity curves generated by the OBMI electrode pairs. Structural orientations for these computed dips (Track 26) are depicted as black 'arrows' or 'tadpoles', in which each arrow consists of a dot, positioned horizontally to show the angle of dip (0–90°) and the direction of the arrow denotes the dip direction (azimuth). Filled dip symbols have a greater level of quality than those with no fill. A manual analysis was also performed on a workstation to check the computed dips and also to fill in depth gaps. The manually selected dips are denoted by green tadpoles. Also depicted in Track 26 (Fig. 1) are 'rose diagrams' or 'fan plots' for the computed dips, with each circular (green) plot graphically representing the sedimentary bed boundary structural orientations over a 50 ft (~15.2 m) portion of the borehole whose boundaries are shown by green diamonds in the center of the plot.

5.27. Track 27

Rt scanner bed boundary true dip

As discussed in Track 5 (Fig. 1), the Rt Scanner tool on the Platform Express (Run-1) has six triaxial arrays, each containing three co-located coils making oriented resistivity measurements at various depths into the formation. The Rt Scanner-derived three-dimensional resistivity model of the near-borehole formation was analyzed on a workstation to identify and characterize sedimentary bed boundaries. Structural orientations at three specific depths (39 inches or ~99.1 cm, 54 inches or ~137.2 cm, and 72 inches or

~182.9 cm) into the borehole wall are depicted in Track 27 (Fig. 1) as 'arrows' or 'tadpoles', in which each arrow consists of a dot, positioned horizontally to show the angle of dip (0–90°) and the direction of the arrow denotes the dip direction (azimuth) at the referenced depth in the formation as indicated by the color of the entire tadpole. The color of the tadpole dot reflects the number of bed boundary measurements used to generate each tadpole. Also depicted in Track 27 (Fig. 1) are 'rose diagrams' or 'fan plots', with each circular (green) plot graphically representing the sedimentary bed boundary structural orientations at 72 inches (~182.9 cm) into the formation over the same 50 ft (~15.2 m) portion of the borehole as was computed for Track 26.

5.28. Track 28

Oil-base microimager tool (OBMI) static image

As previously discussed in the description of Track 25 (Fig. 1), the Oil-Base Microimager Tool (OBMI) (Run-4) produces images of the microresistivity character of the borehole wall that can be used for detailed sedimentological and structural interpretations. It is also possible to use the OBMI log to produce high-resolution electrical images of gas hydrates.

To further assess the nature of in situ gas hydrate occurrences in the Mount Elbert well, the OBMI image was reprocessed and statically normalized such that the entire log was treated as one unit and the microresistivities were placed into 42 separate color shades ranging from yellow to black. Therefore, any zones within the log with the same shade of color will have similar resistivities, unlike the dynamic normalization presentation. In comparison to the 'dynamic' processed OBMI log display in Track 25 (Fig. 1), the 'static' processed OBMI display in Track 28 (Fig. 1) is a less detailed image of the formation; but the gas-hydrate-bearing sections in units C and D can be readily identified.

5.29. Track 29

Cored section

The Mount Elbert well was continuously cored within the depth interval from 1990 ft (606.5 m) to 2494 ft (760.1 m) using the Reed Hycalog *Corion* wireline-retrievable coring system. A total of 23 cores (430 ft or 131 m of core) were recovered as depicted in Track 29 (Fig. 1). The core sections shown in white depict the portion of the core not recovered.

5.30. Track 30

Standard gamma ray (0–150 API)

The standard gamma ray log is the total natural gamma ray count measured by the Hostile Natural Gamma Ray Sonde (HNGS) (Run-5).

Core gamma ray (0–150 API)

After the completion of field operations, the Mount Elbert cores were shipped to Anchorage, Alaska for storage and further analysis. A core-gamma ray scan device was used to obtain a 'core gamma ray log', which was compared to the downhole acquired gamma ray log to help calibrate the log-to-core depths (Rose et al., 2011). Based on the review and analysis of the core based data (e.g., lithostratigraphic composite log, core gamma ray log) versus the borehole wireline log data, a uniform −3 ft (−0.9 m) depth shift was applied to the Mount Elbert core data relative to the wireline log data. The core gamma ray data in this track has been depth shifted. All core data points depicted on the two well log and core montages (Figs. 1 and 2) have been depth shifted to match the downhole wireline log depths.

5.31. Track 31

Measured depth (1900–3000 ft; 579.1–914.4m)

The subsurface depths used in this display are measured from the rotary kelly bushing (RKB) on the drilling rig, which was located 55.18 ft (16.8 m) above sea level. The original well log data was recorded in feet and later converted to meters as depicted in Track 31 (Fig. 1).

6. Mount Elbert gas hydrate reservoir properties – acoustic well log and core montage

The well log and core data described in this section are displayed in Fig. 2 (available online at JMPG). All of the acoustic log data, unless otherwise noted, were depth shifted to match the log data in Fig. 1. The following descriptions are by tracks, labeled T1 through T24 in Fig. 2.

6.1. Tracks 1-2

Tracks 1 and 2 in Fig. 2 are the same as Tracks 1 and 2 in Fig. 1; they have been included in Fig. 2 to allow cross referencing between the two montages.

6.2. Track 3

Track 3 in Fig. 2 is nearly the same as Track 3 in Fig. 1; however, in Fig. 2 the standard resolution density standoff log has been removed and the measured cable speed log (CS) from the Dipole Shear Sonic Imager (DSI) tool run (Run-4) has been substituted. The subsurface depths used in this display are measured from the rotary kelly bushing (RKB) on the drilling rig, which was located 55.18 ft (16.8 m) above sea level. The original well log data was recorded in feet and later converted to meters as depicted in Track 24 (Fig. 2).

6.3. Track 4

Track 4 in Fig. 2 is nearly the same as Track 4 in Fig. 1. In Fig. 2, however, the standard caliper log has been replaced with two orthogonal calipers (Caliper-1 and Caliper-2) as measured with the four-arm Oil-Base Microimager Tool (OBMI) (Run-4). Track 4 (Fig. 2) also includes a plot of the 'Pad-1' azimuth orientation from the General Purpose Inclinometry Tool (GPIT) on the OBMI log run (Run-4).

6.4. Tracks 5–6

Tracks 5 and 6 in Fig. 2 are the same as Tracks 5 and 6 in Fig. 1.

6.5. Track 7

Track 7 in Fig. 2 contains a collection of well logs and core data values that also appear in Tracks 18 and 21 of Fig. 1. In Track 7 of Fig. 2, red hachures have been added to the 'crossover' between the plot of the total CMR and ELAN total porosity, which depicts the gas hydrate bulk volume (BV). The ELAN total porosity is the same as the ELAN porosity in Track 21 of Fig. 1 except it also includes the clay-bound water.

6.6. Track 8

The CMR-DEN gas hydrate saturation curve is the same as that depicted in both Tracks 14 and 15 of Fig. 1.

Table 2
Response equations (expected well log values) for the each of the mineral phases (listed along the top of the table) considered in the ELAN-Plus mineral modeling effort (Fig. 1, Track 9). The weight percent of each component are listed ranging from 0 to 1, with 1 equal to unity or 100%.

ELAN input log data	Water	Coal	Hydrate	Chlorite	Illite	Pyrite	Carbonate	Quartz
Density (g/cm^3)	1.006	1.24	0.91	2.81	2.61	4.99	2.61	2.65
Neutron porosity (%)	1	0.7	1.06	0.58	0.45	0.008	0	-0.021
Iron – Fe (weight %)	0	0	0	0.21	0.05	0.466	0.001	0
Quartz (weight %)[a]	0	0	0	0	0	0	0	1
Carbonate (weight %)[a]	0	0	0	0	0	0	1	0
Pyrite (weight %)[a]	0	0	0	0	0	1	0	0
Clay (weight %)[a]	0	0	0	1	1	0	0	0
Coal (weight %)[a]	0	1	0	0	0	0	0	0
Hydrate (weight %)[b]	0	0	1	0	0	0	0	0

[a] SepctroLith derived log values (assigned values).
[b] Calculated outside of ELAN (assigned values).

6.7. Track 9

Track 9 in Fig. 2 is the same as Track 13 in Fig. 1.

6.8. Track 10

Track 10 in Fig. 2 is the same as Track 28 in Fig. 1.

6.9. Track 11

Track 11 in Fig. 2 is the same as Track 26 in Fig. 1.

6.10. Track 12

Compressional-wave velocity (5000–12,000 ft/s; approximately 1.5–3.7 km/s)

The compressional-wave velocity log depicted in Track 12 (Fig. 2) has been derived from the compressional-wave coherence plot in Track 14 (Fig. 2), which was obtained by the Dipole Shear Sonic Imager (DSI) (Run-4). The high compressional-wave velocities recorded in unit C (2132–2186 ft; 649.8–666.3 m) and unit D (614.4–627.9 m; 2016–2060 ft) have been attributed to the occurrence of in situ gas hydrate.

Fast shear-wave velocity (1000–8000 ft/s; approximately 0.3–2.4 km/s)

The shear-wave velocity log (in the fast shear-wave direction) depicted in Track 12 (Fig. 2) has been derived from the shear-wave coherence plot in Track 15 (Fig. 2), which was obtained by the Dipole Shear Sonic Imager (DSI) (Run-4). The high shear-wave velocities recorded in unit C (2132–2186 ft; 649.8–666.3 m) and unit D (2016–2060 ft; 614.4–627.9 m) have been attributed to the occurrence of in situ gas hydrate. The methods used to derive the fast and slow shear-wave velocities are further reviewed below in the descriptions of Tracks 17, 18, and 19 (Fig. 2).

Stoneley-wave velocity (500–4000 ft/s; approximately 0.2–1.2 km/s)

The Stoneley-wave velocity log depicted in Track 12 (Fig. 2) has been derived from the Stoneley-wave coherence plot in Track 16 (Fig. 2), which was obtained by the Dipole Shear Sonic Imager (DSI) log run (Run-4).

6.11. Track 13

Compressional-wave slowness (40–180 micro-sec/ft; approximately 131–591 micro-sec/m)

The compressional-wave slowness log depicted in Track 13 (Fig. 2) has been derived from the compressional-wave coherence plot in Track 14 (Fig. 2), which was obtained by the Dipole Shear Sonic Imager (DSI) (Run-4).

Shear-wave slowness of fast shear waves (150–850 micro-sec/ft; approximately 492–2789 micro-sec/m)

The shear-wave slowness (in the fast shear-wave direction) log depicted in Track 13 (Fig. 2) has been derived from the shear-wave coherence plot in Track 15 (Fig. 2), which was obtained by the Dipole Shear Sonic Imager (DSI) (Run-4). The methods used to derive the fast and slow shear-wave transit-times are further reviewed below in the descriptions of Tracks 17, 18, and 19 (Fig. 2).

Stoneley-wave slowness (250–600 micro-sec/ft; approximately 820–1969 micro-sec/m)

The Stoneley-wave slowness log depicted in Track 13 (Fig. 2) has been derived from the Stoneley-wave coherence plot in Track 16 (Fig. 2), which was obtained by the Dipole Shear Sonic Imager (DSI) (Run-4).

6.12. Track 14

Coherence plot of compressional-wave slowness (40–280 micro-sec/ft; approximately 131–918 micro-sec/m)
Compressional-wave slowness (40–280 micro-sec/ft; approximately 131–918 micro-sec/m)

Track 14 displays the compressional-wave slowness as measured by the Dipole Shear Sonic Imager (DSI) (Run-4). The compressional-wave slowness has been extrapolated from the statistical overlay of the compressional-wave coherence plot from the DSI monopole array. This data has not been depth shifted.

6.13. Track 15

Coherence plot of fast shear-wave slowness (112–772 micro-sec/ft; approximately 367–2533 micro-sec/m)
Fast shear-wave slowness (112–772 micro-sec/ft; approximately 367–2533 micro-sec/m)

Track 15 displays the fast shear-wave slowness (in the fast shear-wave direction) measured by the Dipole Shear Sonic Imager (DSI) (Run-4). In Track 15 the fast shear-wave receiver slowness has been extrapolated from the statistical overlay of the fast shear-wave slowness time coherence plot from the DSI monopole array. The methods used to derive the fast and slow shear-wave slowness are further reviewed below in the descriptions of Tracks 17, 18, and 19 (Fig. 2). This data has not been depth-shifted.

6.14. Track 16

Coherence plot of Stoneley-wave slowness (200–900 micro-sec/ft; approximately 656–2953 micro-sec/m)
Stoneley-wave slowness (200–900 micro-sec/ft; approximately 656–2953 micro-sec/m)

Track 16 displays the Stoneley-wave slowness measured by the Dipole Shear Sonic Imager (DSI) (Run 4). In Track 16 (Fig. 2) the Stoneley-wave slowness has been extrapolated from the statistical overlay of the Stoneley-wave coherence plot from the DSI monopole array. This data has not been depth-shifted.

6.15. Tracks 17 and 18

Minimum cross-acoustic energy (ratio, 0–100)
Maximum cross acoustic energy (ratio, 0–100)
Fast-shear azimuth (−90 to 90 deg)
Fast-shear azimuth − minimum (−90 to 90 deg)
Fastshear azimuth − maximum (−90 to 90 deg)

The Dipole Shear Sonic Imager log (DSI) (Run-4) allowed for the complete analysis of the shear wave acoustic anisotropy of the hydrate-bearing sedimentary section at Mount Elbert. Cross-dipole acoustic-logging tools can measure shear-waves in both fast and slow formations, as well as characterize the shear anisotropy of the formation using traditional time-domain processing techniques. Acoustic anisotropy can be characterized as either intrinsic (i.e., bedding, shales, aligned fractures) or stress-induced. Recently it has been shown that frequency domain processing of cross-dipole data (i.e., slowness-frequency analysis or dispersion analysis) enhances the interpretation of the data by distinguishing intrinsic from stress-induced anisotropy (Plona and Kane, 2005). Dispersion analysis augments traditional time-based semblance processing to yield a more complete characterization of the formation. Schlumberger Well Logging Services used standard frequency-domain processing techniques to evaluate the isotropic/anisotropic acoustic nature of the formations at the Mount Elbert well site with the recorded Dipole Shear Sonic Imager log data (DSI) (Run-4). This study has shown that the gas-hydrate-bearing sandstone units in the Mount Elbert well have low compressional-wave and shear-wave slownesses (fast sound speeds) and behave in a homogeneous and isotropic manner. In contrast, the water-bearing sandstone section exhibits much higher compressional-wave and shear-wave slownesses (slow sound speeds), stress-induced anisotropy, and mechanical damage around the wellbore, as indicated by additional radial acoustic slowness gradients.

In Track 17 (Fig. 2), the relative acoustic energy level as seen by the receivers on the DSI tool are plotted for the minimum and maximum shear-wave slowness directions. Note that within gas-hydrate-bearing sandstone intervals (unit C 2132–2186 ft; 649.8–666.3 m and unit D 2016–2060 ft; 614.4–627.9 m), the acoustic energies as seen by the DSI are relatively similar in both the minimum and maximum shear-wave slowness directions, with a slightly greater difference in the unit C hydrate-bearing section. In the water-bearing sandstone intervals, such as unit B (2480–2660 ft; 775.9–810.7 m), the DSI measured acoustic energies differ significantly between the minimum and maximum shear-wave slowness directions (highlighted in green).

In Track 18 (Fig. 2), the azimuth of the fast shear-wave slowness directions have been plotted along with the expected uncertainty in the fast shear-wave slowness direction (shaded in gray).

6.16. Track 19

Shear-wave slowness in fast direction (40–540 micro-sec/ft; approximately 131–1772 micro-sec/m)
Shear wave slowness in slow direction (40–540 micro-sec/ft; approximately 131–1772 micro-sec/m)
Slowness-based anisotropy (relative scale, 0–100%)
Time-based anisotropy (relative scale, 0–100%)

The Dipole Shear Sonic Imager log (DSI) (Run-4) was used to analyze the shear wave acoustic anisotropy of the gas-hydrate-bearing sediments at the Mount Elbert site as shown in the description of Tracks 17 and 18 (Fig. 2). Track 19 (Fig. 2) includes plots of the DSI-derived shear-wave slownesses in both the fast and slow directions. Track 19 also includes a plot of the relative slowness anisotropy (shaded in green), which derived with the following equation:

$$\text{Slowness Anisotropy} = \frac{\left(DT_{slow} - DT_{fast}\right)}{\left(DT_{slow} + DT_{fast}\right)/2}100 \tag{7}$$

where DT is shear slowness. Time-based anisotropy is calculated by

$$\text{Time Anisotreopy} = \frac{TT_{diff}}{TT_{fast}}100 \tag{8}$$

where TT_{diff} is the arrival time difference between fast and slow shear waves; TT_{fast} is the fast shear arrival time.

6.17. Tracks 20 and 21

Stoneley waveform (0–20,440 microsec)
Borehole diameter (OBMI caliper 1) (4–14 inches; approximately 10.2–35.6 cm)
Stoneley reflection coefficient-up (ratio, 0.0–0.5)
Stoneley reflection coefficient-down (ratio, 0.0–0.5)

Track 21 (Fig. 2) shows the complete Stoneley waveform acquired by the Dipole Shear Sonic Imager (DSI) (Run-4) in the Mount Elbert well. In Tracks 20 and 21 (Fig. 2), the low-frequency reflected Stoneley-wave mode has been used to locate Stoneley-wave reflections of permeable fractures intersecting the borehole. Attenuation of direct Stoneley-waves in a borehole is due to fractures cross-cutting the borehole and fluid flow into the permeable fracture, a mechanism which also gives rise to reflected Stoneley-waves. The Stoneley-wave data processing in Tracks 20 and 21 (Fig. 2) involved computation of the Stoneley-wave reflectivity response using the measured direct and reflected Stoneley-wave arrivals. A least-squares fit to the arrival time of the reflected-wave arrivals was used to estimate the well depth of the permeable fractures. The sonic waveform in Track 21 (Fig. 2) is dominated by numerous large amplitude reflections, possibly indicating the presence of significant fractures, flagged on the plot of the up (red) and down (green) Stoneley reflection coefficient logs in Track 20 (Fig. 2); however, irregularities in the shape and size of the borehole can adversely affect the Stoneley-wave arrivals. The borehole diameter log (caliper) has been added to Track 21 (Fig. 2) to highlight zones in which borehole conditions may affect the Stoneley-wave analysis. The Stoneley waveform (Track 21) has not been depth-shifted.

6.18. Track 22

Poisson's ratio (ratio, 0–0.5)

Track 22 (Fig. 2) contains a well log of the Poisson's ratio (σ) computed from the Dipole Shear Sonic Imager (DSI) (Run-4). The

Poisson's ratio (σ) log in Track 22 was calculated from the DSI-derived compressional- and fast shear-wave velocities (*Vp* and *Vs*) and the following relation, developed by Gassmann (1951):

$$\sigma = \frac{\frac{1}{2}\left[\frac{V_P}{V_S}\right]^2 - 1}{\left[\frac{V_P}{V_S}\right]^2 - 1} \tag{9}$$

Young's modulus (0–2.5 MPa)

Track 22 (Fig. 2) also contains a log display of Young's modulus (E) calculated from the compressional- and shear-wave velocities (*Vp* and *Vs*) and the density log using the following relations developed by Gassmann (1951):

$$E = \frac{9KG}{3K + G} \tag{10}$$

where *K* is the bulk modulus, given by the following relation:

$$V_P = \left[\frac{(K + 4G/3)}{\rho_b}\right]^{\frac{1}{2}} \tag{11}$$

where *G* (the well-log-calculated shear modulus) is derived from the Dipole Shear Sonic Imager (DSI) (Run-4) and ρ_b (the bulk-density of the formation) was measured by the Platform Express (PEX) (Run-1).

Shear modulus (0–2.5 MPa)

Track 22 (Fig. 2) also contains a well log of the shear modulus (*G*) calculated from the shear-wave velocities (*Vs*), the density log, and the following relation developed by Gassmann (1951):

$$V_S = \left[\frac{G}{\rho_b}\right]^{\frac{1}{2}} \tag{12}$$

where the bulk-density (ρ_b) of the formation is obtained from the densities recorded by the Platform Express (Run-1).

6.19. Track 23

Vp/Vs (ratio, 1.0–3.5)

The presence of free-gas in contact with gas hydrate occurrences is an important consideration when designing possible production scenarios and assessing drilling hazards. Measured compressional-wave/shear-wave velocity ratios less than ~1.9 are often indicative of free-gas-bearing sediments. As shown in Track 23 (Fig. 2), however, the log measured compressional-wave/shear-wave velocity ratios measured by the Dipole Shear Sonic Imager (DSI) (Run-4), are uniformly higher than the 1.9 threshold.

6.20. Track 24

Measured depth (1900–3000 ft; 579.1–914.4 m)

The subsurface depths used in this display are measured from the rotary kelly bushing (RKB) on the drilling rig, which was located 55.18 ft (16.8 m) above sea level. The original well log data was recorded in feet and later converted to meters as depicted in Track 24 (Fig. 2).

7. Summary

Analysis of downhole logs has confirmed the occurrence of two relatively thick gas-hydrate-bearing stratigraphic sections units (unit C 2132–2186 ft [649.8–666.3 m] and unit D 2016–2060 ft [614.4–627.9 m]) within the BPXA-DOE-USGS Mount Elbert Gas Hydrate Stratigraphic Test Well. The downhole well log and core data has yielded a wealth of geologic and engineering data from the Mount Elbert gas hydrate prospect. High resolution borehole surveys have revealed that the gas hydrates of the Mount Elbert well appear to be pore filling constituents within relatively high quality sandstone reservoir rocks. Porosities of the gas-hydrate-bearing reservoir rocks, derived by various well log and core analyses, range from ~35 % to ~40 %. Gas hydrate saturations within the gas-hydrate-bearing units of the Mount Elbert well, calculated by various well log methods reviewed in this study, are very high with average values ranging from ~50 to ~78%.

References

Amer, A., Alexander, S., 2005. Interpreting the depositional facies of the Upper Garif Fluvial System using oil-based mud images: a case study in Central Oman. Society of Petroleum Engineers Paper 95584, 13. p.

Anderson, B., Hancock, S., Wilson, S., Collett, T., Boswell, R., Hunter, R., 2011. Formation pressure testing at the Mount Elbert Gas Hydrate Stratigraphic Test Well, Alaska North Slope: Operational summary, history matching, and interpretations. Journal of Marine and Petroleum Geology 28 (2), 478–492.

Bird, K.J., 1998. Geographic and geologic setting, Chapter GG. In: The Oil and Gas Resource Potential of the Arctic National Wildlife Refuge 1002 Area, Alaska, by ANWR Assessment Team: U.S. Geological Survey Open-File Report 98-34, Version 1.0, p. GG1-GG51, CD-ROM. http://pubs.usgs.gov/of/1998/ofr-98-0034/GG.pdf.

Collett, T.S., 1993. Natural gas hydrates of the Prudhoe Bay and Kuparuk River area, North Slope, Alaska. American Association of Petroleum Geologists Bulletin 77 (5), 793–812.

Collett, T.S., 1998. Well log characterization of sediment porosities in gas-hydrate-bearing reservoirs. In: Proceedings of the 1998 Annual Technical Conference and Exhibition of the Society of Petroleum Engineers, September 27–30, 1998, New Orleans, Louisiana, USA. Society of Petroleum Engineers, Houston, Texas, p. 12.

Collett, T.S., Lee, M., 2005. Electrical resistivity well-log analysis of gas hydrate saturations in the JAPEX/JNOC/GSC et al. Mallik 5L-38 well. In: Dallimore, S.R., Collett, T.S. (Eds.), Scientific Results from the Mallik 2002 Gas Hydrate Production Research Well Program, Mackenzie Delta, Northwest Territories, Canada. Geological Survey of Canada Bulletin 585, 8. two CD-ROM set.

Collett, T.S., Lewis, R.E., Dallimore, S.R., 2005. JAPEX/JNOC/GSC et al. Mallik 5L-38 gas hydrate production research well downhole well-log and core montages. In: Dallimore, S.R., Collett, T.S. (Eds.), Scientific Results from the Mallik 2002 Gas Hydrate Production Research Well Program, Mackenzie Delta, Northwest Territories, Canada. Geological Survey of Canada Bulletin 585, 23. two CD-ROM set.

Gassmann, F., 1951, Elasticity of porous media: uber die elastizitat poroser medien, Vierteljahrsschrift der Naturforschenden Gesselschaft in Zurich, Heft 1.

Guerin, G., Goldberg, D., 2005. Sonic attenuation in the JAPEX/JNOC/GSC et al. Mallik 5L-38 gas hydrate research well. In: Dallimore, S.R., Collett, T.S. (Eds.), Scientific Results from the Mallik 2002 Gas Hydrate Production Research Well Program, Mackenzie Delta, Northwest Territories, Canada. Geological Survey of Canada Bulletin 585, 9. two CD-ROM set.

Herron, M.W., 1987. Estimating the intrinsic permeability of clastic sediments from geochemical data. In: Proceedings of the Society of Professional Well Log Analyst Annual Logging Symposium, June 29–July 2, 1987, Paper HH, 23p.

Herron, S.L., Herron, M.W., 1996. Quantitative lithology: An application for open and cased hole spectroscopy. In: Proceedings of the Society of Professional Well Log Analyst Annual Logging Symposium, June 16–19, 1996, Paper E, 14p.

Herron, S.L., Herron, M.W., 2000. Application of nuclear spectroscopy logs to the derivation of formation matrix density. In: Proceedings of the Society of Professional Well Log Analyst Annual Logging Symposium, June 4–7, 2000, Paper JJ, 12p.

Horkowitz, J., Crary, S., Ganesan, K., Heidler, R., Luong, B., Morley, J., Petricola, M., Prusiecki, C., Speier, P., Poitzsch, M., Scheibal, J.R., Hashem, M., 2002. Applications of a new magnetic resonance logging-while-drilling tool in a Gulf of Mexico deepwater development well. In: Proceedings of the Society of Professional Well Log Analyst Annual Logging Symposium, June 2–5, 2002, Paper EEE, 14p.

Hunter, R., Collett, T., Boswell, R., Anderson, B., Digert, S., Pospisil, G., Baker, R., Weeks, M., 2011. Mount Elbert Gas Hydrate Stratigraphic Test Well, Alaska North Slope: Overview of scientific and technical program. Journal of Marine and Petroleum Geology 28 (2), 295–310.

Kleinberg, R.L., Flaum, C., Collett, T.S., 2005. Magnetic Resonance Log of JAPEX/JNOC/GSC et al. Mallik 5L-38 gas hydrate production research well: gas hydrate saturation, growth habit, and relative permeability. In: Dallimore, S.R., Collett, T.S. (Eds.), Scientific Results from the Mallik 2002 Gas Hydrate Production Research Well Program, Mackenzie Delta, Northwest Territories, Canada. Geological Survey of Canada Bulletin 585, 10. two CD-ROM set.

Lee, M., Agena, W., Collett, T., Inks, T., 2011. Pre- and post-drill comparison of the Mount Elbert gas hydrate prospect. Alaska North Slope. Journal of Marine and Petroleum Geology 28 (2), 578–588.

Lee, M.W., Collett, T.S., 2005. Assessments of gas hydrate concentrations estimated from sonic logs in the Mallik 5L-38 gas hydrate research production well, Northwest Territories, Canada. In: Dallimore, S.R., Collett, T.S. (Eds.), Scientific Results from the Mallik 2002 Gas Hydrate Production Research Well Program, Mackenzie Delta, Northwest Territories, Canada. Geological Survey of Canada Bulletin 585, 10. two CD-ROM set.

Lee, M.W., Collett, T.S., 2011. In-situ gas hydrate hydrate saturation estimated from various well logs at the Mount Elbert Gas Hydrate Stratigraphic Test Well, Alaska North Slope. Journal of Marine and Petroleum Geology 28 (2), 439–449.

Lee, M.W., Hutchinson, D.R., Collett, T.S., Dillon, W.P., 1996. Seismic velocities for hydrate-bearing sediments using weighted equation. Journal of Geophysical Research 101 (B9), 20347–20358.

Lorenson, T.D., Collett, T.S., Hunter, R.B., 2011. Gas geochemistry of the Mount Elbert Gas Hydrate Stratigraphic Test Well, Alaska North Slope: Implications for gas hydrate exploration in the Arctic. Journal of Marine and Petroleum Geology 28 (2), 343–360.

Mayer, C., Sibbit, A., 1980. Global, A new approach to computer-processed log interpretation, Society of Professional Engineers 55th Annual Conference, September 21-24, 1980, SPE 9341, 14p.

Molenaar, C.M., Bird, K.J., Kirk, A.R., 1987. Cretaceous and Tertiary stratigraphy of northeastern Alaska. In: Tailleur, I., Weimer, P. (Eds.), Alaskan North Slope Geology, v. 1: Bakersfield, California, Pacific Section, Society of Economic Paleontologists and Mineralogists and Alaska Geological Society, pp. 513–528.

Plona, T.J., Kane, M.R., 2005. Anisotropic stress analysis from downhole acoustic logs in the JAPEX/JNOC/GSC et al., Mallik 5L-38 gas hydrate production research well. In: Dallimore, S.R., Collett, T.S. (Eds.), Scientific Results from the Mallik 2002 Gas Hydrate Production Research Well Program, Mackenzie Delta, Northwest Territories, Canada. Geological Survey of Canada Bulletin 585, 8. two CD-ROM set.

Quirein, J., Kimminau, S., LaVigne, J., Singer, J., Wendel, F., 1986. A coherent framework for developing and applying multiple formation evaluation models. Transactions of the Society of Professional Well Log Analysts 27th Annual Logging Symposium, Paper DD.

Rose, K., Boswell, R., Collett, T., 2011. Mount Elbert Gas Hydrate Stratigraphic Test Well, Alaska North Slope: Coring operations, core sedimentology, and lithostratigraphy. Journal of Marine and Petroleum Geology 28 (2), 311–331.

Serra, O., 1984. Fundamentals of Well-Log Interpretation. In: Developments in Petroleum Science, vol. 1. Elsevier Publishing, Amsterdam, The Netherlands, pp. 196–197.

Sun, Y.-F., Goldberg, D., 2005. Analysis of electromagnetic propagation tool response in gas-hydrate-bearing formations. In: Dallimore, S.R., Collett, T.S. (Eds.), Scientific Results from the Mallik 2002 Gas Hydrate Production Research Well Program, Mackenzie Delta, Northwest Territories, Canada. Geological Survey of Canada Bulletin 585, 8. two CD-ROM set.

Sun, Y., Goldberg, D., Collett, T., Hunter, R., 2011. High-resolution well-log derived dielectric properties of gas-hydrate-bearing sediments, Mount Elbert Gas Hydrate Stratigraphic Test Well, Alaska North Slope. Journal of Marine and Petroleum Geology 28 (2), 450–459.

Tomaru, H., Matsumoto, R., Chen, Y.F., Lu, H., Clark, I.D., 2005. Evolution of a gas hydrate system as recorded by oxygen and hydrogen isotopes of the interstitial waters of the JAPEX/JNOC/GSC et al. Mallik 5L-38 gas hydrate production research well. In: Dallimore, S.R., Collett, T.S. (Eds.), Scientific Results from the Mallik 2002 Gas Hydrate Production Research Well Program, Mackenzie Delta, Northwest Territories, Canada. Geological Survey of Canada Bulletin 585, 12. two CD-ROM set.

Torres, M., Collett, T., Rose, K., Sample, J., Agena, W., Rosenbaum, E., 2011. Pore Fluid Geochemistry from the Mount Elbert Gas Hydrate Stratigraphic Test Well, Alaska North Slope. Journal of Marine and Petroleum Geology 28 (2), 332–342.

Tréhu, A.M., Long, P.E., Torres, M.E., et al., 2004. Three-dimensional distribution of gas hydrate beneath southern Hydrate Ridge: constraints from ODP Leg 204. Earth and Planetary Science Letters 222, 845–862.

Winters, W., Walker, M., Hunter, R., Collett, T., Boswell, R., Torres, M., Patil, S., Dandekar, A., 2011. Physical properties of sediment from the Mount Elbert Gas Hydrate Stratigraphic Test Well, Alaska North Slope. Journal of Marine and Petroleum Geology 28 (2), 361–380.